

A study on Scintillating Fiber tracker optimisation for the LHCb upgrade

Alessio Piucci ¹, Andrea Mogini ², Sevda Esen ¹, Thomas Nikodem ¹

¹ *Physikalisches Institute, Ruprecht-Karls-Universität Heidelberg, Heidelberg, Germany*

² *LPNHE, Paris, France*

Abstract

New tracking stations made from scintillating fibres are designed as a part of the LHCb Upgrade to provide the tracking capabilities in the data-taking environment foreseen after Run II. Due to the higher track multiplicity and higher total integrated radiation dose, larger inefficiencies are found in the simulation compared to the current tracker. This note presents the optimisation studies and proposals which would improve the reconstruction efficiency in the three stations of the scintillating fiber tracker.

Contents

1	Introduction	1
2	Current tracking algorithms	2
2.1	Forward tracking	2
2.2	Seeding algorithm	5
2.3	Performances	5
3	Optimization studies	5
3.1	<i>y</i> Segmentation	6
3.1.1	Simulation	7
3.1.2	Optimization of the tracking algorithms	7
3.1.3	Results	9
3.2	Additional <i>x</i> layers	9
3.2.1	Simulation	10
3.2.2	Forward algorithm optimisation and performances	11
3.2.3	Seeding algorithm adaptation and performances	14
3.3	Beam hole and layer size	16
3.3.1	Simulation	17
3.3.2	Results	19
4	Conclusions	22
	References	23

1 Introduction

The LHCb detector [1,2] is a single-arm forward spectrometer covering the pseudorapidity range $2 < \eta < 5$, designed for the study of particles containing b or c quarks. For the upgrade, several subdetectors will be modified, including the tracking stations which will be completely replaced [3]. A sketch of the LHCb upgraded detector is shown in Fig. 1.

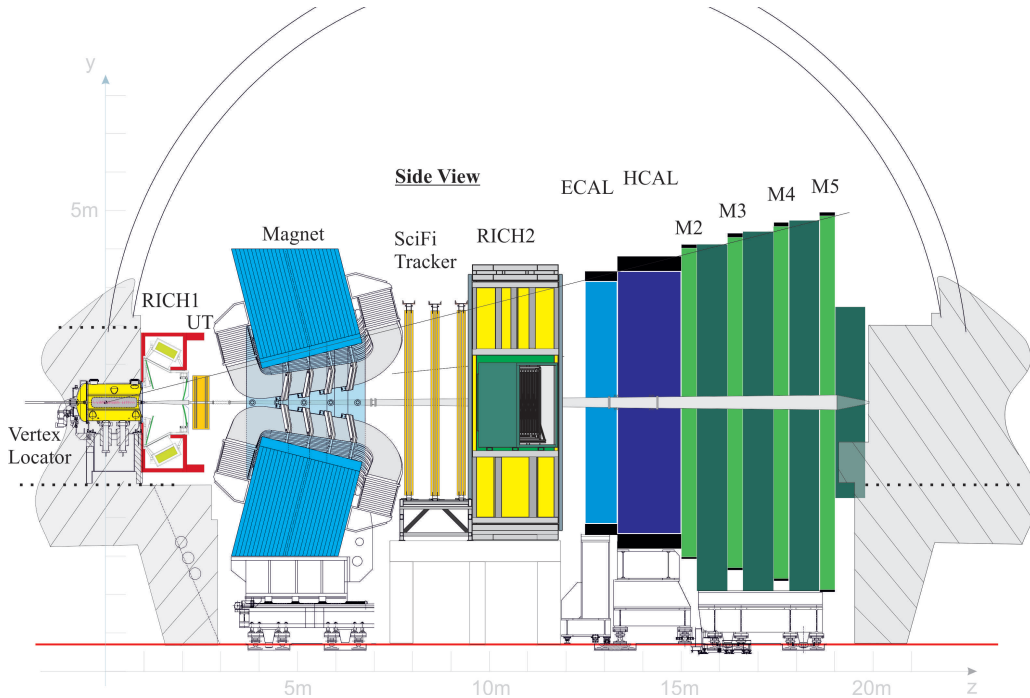


Figure 1: Schematic view of the upgraded LHCb detector.

The large tracking detector downstream of the magnet consists of three stations, T1, T2, T3, as shown in Fig. 2 with mats of scintillating fibres as active material. The detector geometry is described in detail in Ref. [4]. Each station is composed of four layers ($x-u-v-x$). In the first and fourth layer of each station, fibres are vertically oriented to give the x coordinate of the track at that position, while in the second and third layers the fibers have a $\pm 5^\circ$ angle with the y axis of the laboratory frame, providing the u and v stereo coordinates as shown in Fig. 3. The effects of radiation damage corresponding to 50 fb^{-1} of data-taking are simulated in the events used to evaluate the performance of the scintillating-fibre (SciFi) detector. For these conditions, the expected efficiency to detect a single hit is $\approx 99\%$ [5]. Additional inefficiencies are caused by the dead regions of the detector and the clustering algorithm. Overall, the hit efficiency is $\approx 96\%$ in the simulation. The single hit resolution is $\sim 70 \mu\text{m}$ depending on the number of fibres combined in a cluster. The hit resolution is sufficiently small, as the limiting factor for the momentum resolution is multiple scattering. Nevertheless, the good spatial resolution is an advantage for pattern recognition algorithms for efficient track finding and reducing the number of

21 wrong combinatorics.

22 Several proposals which are made to improve the tracking performance are studied. In
23 order to reduce the amount of fake tracks reconstructed, we study the effect of additional
24 y position information by placing two y -segmented layers in the high occupancy regions of
25 the detector. A second option is to have two additional layers in the inner regions, which
26 can provide better selection of high momentum tracks without reconstructing more fake
27 tracks. Finally, the size and shape of the SciFi beam hole, as well the layer sizes, are
28 studied to optimise the tracking performances accordingly with the mechanical constraints.
29 This note will describe these optimisation studies and results from the current Forward
30 and Seeding tracking algorithms.

31 **2 Current tracking algorithms**

32 Tracks are classified based on the different tracking subdetectors that they traverse as
33 illustrated in Fig. 4. Several tracking algorithms are designed to find all track types
34 effectively. The long tracks are mainly reconstructed by the forward algorithm while the
35 seeding algorithm reconstructs the T tracks. T tracks can later be used to make long
36 tracks by a matching algorithm or downstream tracks by a downstream-tracking algorithm.

37 **2.1 Forward tracking**

38 The forward algorithm [6] uses as input the reconstructed VELO tracks of the event, which
39 provide additional information in the reconstruction process. The output tracks of the
40 forward algorithm are long tracks. They include measurements from at least the VELO
41 and the SciFi detector, and thus provide a precise measurement of the four-vector of the
42 particle.

43 The main idea of the forward algorithm is that a single measurement of the SciFi
44 detector, combined with a VELO track, is enough to determine the trajectory of the
45 particle through the detector. Therefore, for each combination of VELO input track and
46 SciFi measurement an intersection of the hypothetical particle with a plane at a fixed z
47 value (the so-called *reference plane*) is calculated. Measurements belonging to the same
48 particle as the VELO track cluster together on this plane. A sketch of this Hough-like
49 clustering is shown in Fig. 5.

50 In the forward algorithm the clustering is done with all measurements from the x planes
51 which pass a *preselection* stage. In this stage the x -measurement is projected to the nearest
52 u/v plane and it is checked for a consistent measurement in this plane. In particular, a
53 matching of the x hit with at least one hit on the stereo plane is required, within a window
54 which depends on the slope of the VELO track. If the x hit does not match with any
55 stereo hit, it is not used in the Hough-like clustering later. The preselection is important
56 for removing wrong measurements, however, as now two measurements of the particle are
57 required, the hit efficiency is effectively reduced. A missing measurement already in this
58 early reconstruction stage is problematic for all following reconstruction stages; therefore

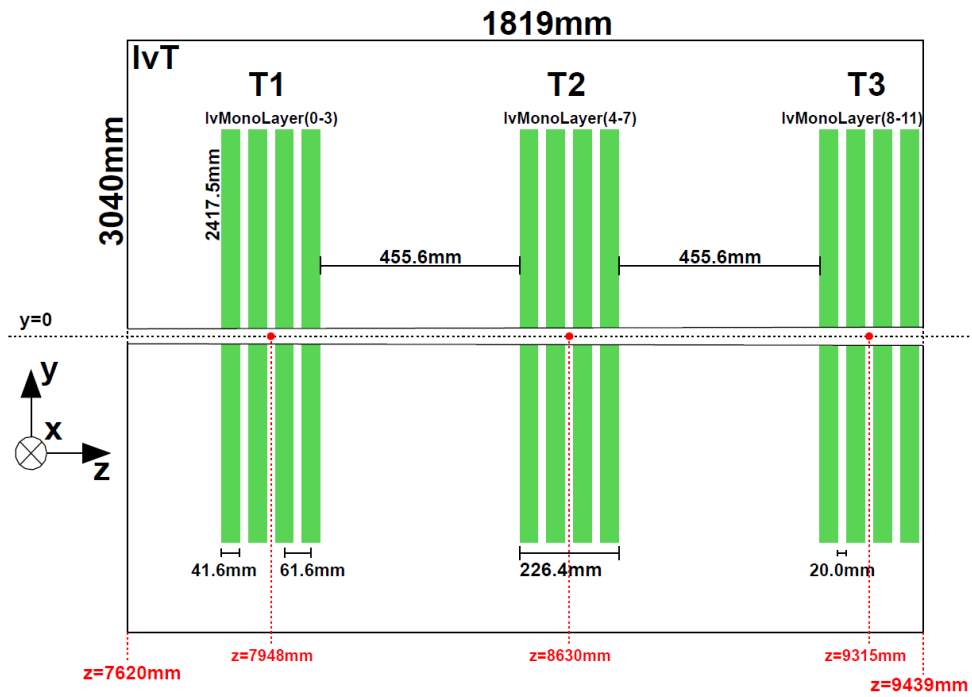


Figure 2: Schematic side view of the SciFi tracking stations.

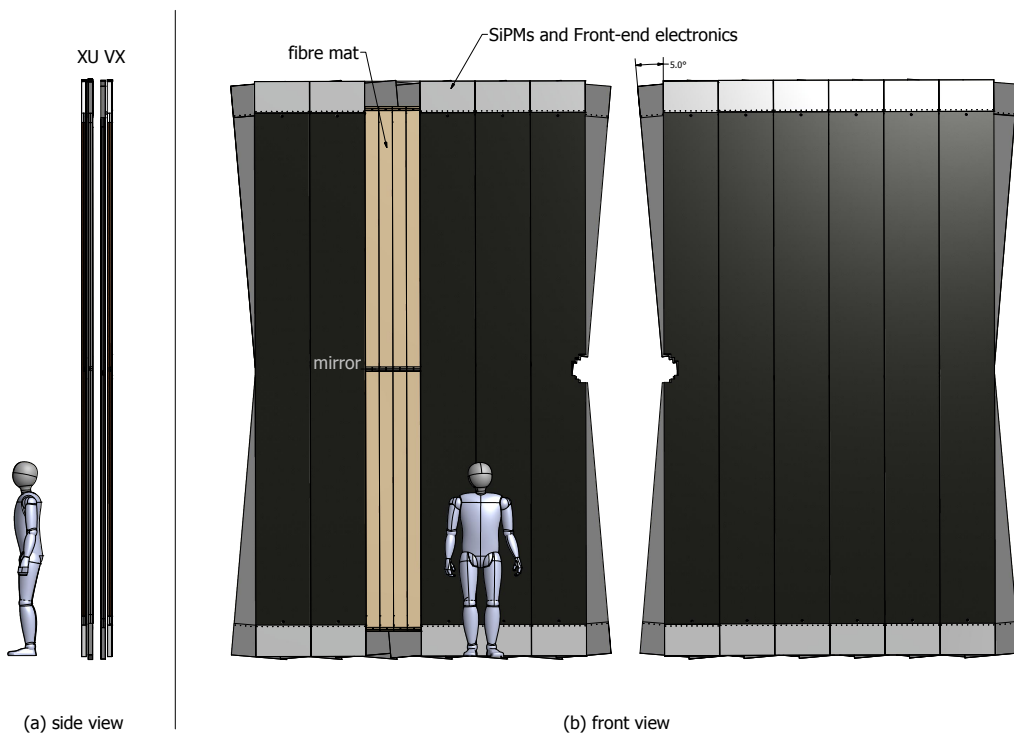


Figure 3: Schematic view of a SciFi station.

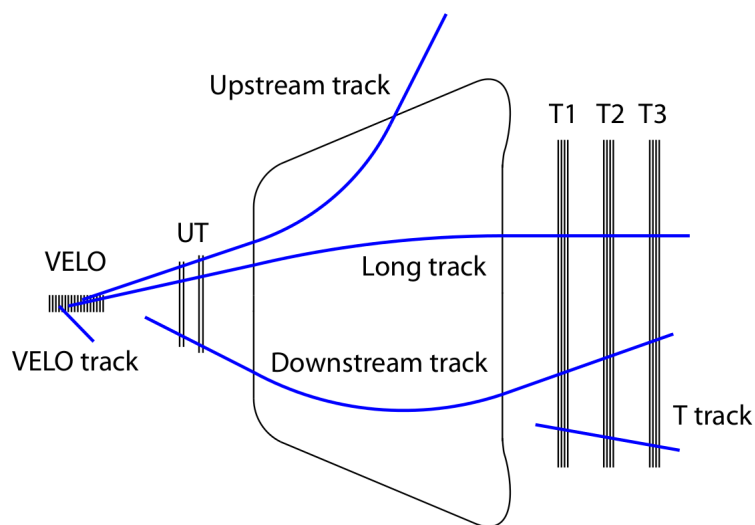


Figure 4: Track types at LHCb.

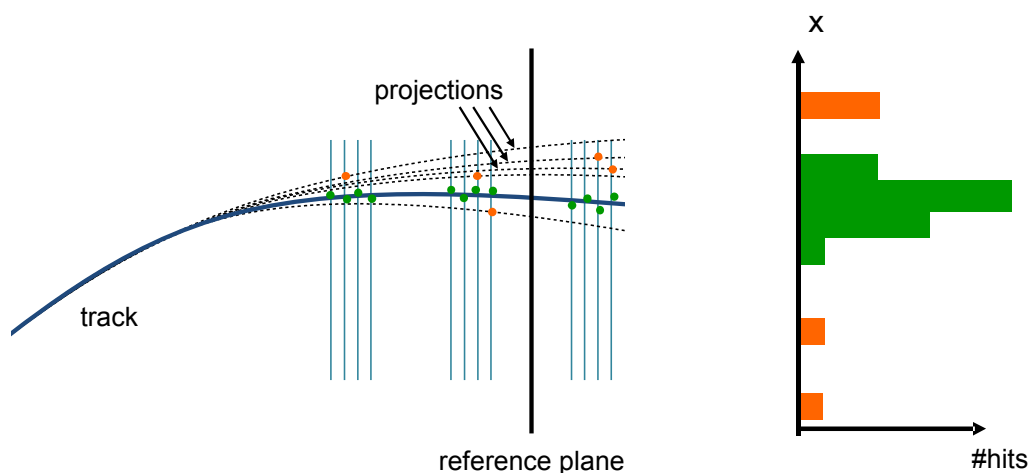


Figure 5: A sketch of the projection of x hits on a reference plane. The green dots are hits which belong to the particle intersecting the detector, represented as a thick blue line. The orange dots are hits from other particles, or from noise sources. The black dotted lines represent projections of single hits to the reference plane. Only hits which belong to the same particle cluster together on the reference plane, on the right [6].

59 this step shows great potential to benefit from an improved detector design.
 60 In the further processing, several χ^2 fits are performed to select the measurements
 61 which match the trajectory best. Afterwards, measurements from u/v planes which are
 62 compatible with the x candidate are searched, and a final χ^2 fit including all measurements
 63 is done. The last stage of the algorithm is a cleanup, which attempts to remove fake tracks
 64 and tracks that are multiply reconstructed.

2.2 Seeding algorithm

The seeding algorithm reconstructs tracks using only hits in the SciFi tracking stations. The algorithm is crucial for the reconstruction of the long lived particles as well as a good indicator of the detector performance since it performs independently from the other sub detectors.

The current seeding algorithm is called hybrid seeding and described in detail in Ref. [7]. The algorithm needs to find the tracks without any prior information which requires many hit combinations to be tested. The current algorithm is designed to reach a good compromise between tracking efficiencies, amount of fake tracks reconstructed and timing. The main idea behind the hybrid seeding is to progressively clean the tracking environment by finding the tracks which are easier to reconstruct first and then looking for the rest using the leftover hits. For each event, using hits in six x -layers, all possible track candidates passing the minimum hit and fit quality requirements are reconstructed. These candidates are later combined with hits in the stereo layers to obtain the full tracks.

In the following, all results pertaining to the seeding algorithm are obtained using the most recent version of the algorithm at the time of each study.

2.3 Performances

The reconstruction efficiency is defined as the ratio between the number of reconstructed tracks which are matched to a *reconstructible* simulated particle, and the total number of simulated reconstructible particles. Particles are considered to be reconstructible if they leave enough hits in the tracking layers as to meet a specific requirement.

Reconstructed track candidates which do not correspond to any simulated particle are called ghosts. T-track ghosts, reconstructed using SciFi measurements, are referred to as *T-ghosts*. Long candidates which are ghosts can be further classified as T-ghost if the reconstructed part in the T stations is a T-ghost, or as *matching ghost* if the VELO and T parts are not ghosts, but they do not correspond to the same simulated particle. Finally, the ghost rate is defined as the ratio of ghost tracks over all reconstructed tracks.

Tracking performances of the forward and hybrid seeding algorithms are summarised in Table 1.

3 Optimization studies

The track reconstruction performances can be improved by increasing the signal-over-background ratio of hits produced in the detector, where signal hits are referred to be the ones produced by particles intersecting the tracking layers, and the background ones come from noise sources of the detector or from spillover events. This can be accomplished by decreasing the detector noise, which is difficult without resulting in lower hit efficiency and consequently in a smaller portion of signal tracks. Another approach is to increase the number of good hits available for the reconstruction, for instance using more tracking

	Forward	Seeding
long	83.8%	90.5%
long, $p > 5 \text{ GeV}/c$	92.1%	94.0%
long, $p > 5 \text{ GeV}/c$, from B	94.5%	
total ghost rate	35.9%	18.3%
T-ghost rate	17.5%	18.3%
matching ghost rate	18.4%	

Table 1: Tracking performances for forward and seeding algorithms. Reconstruction efficiency for long particles and ghost rates are shown. The results are computed over a sample of 5000 simulated $B_s \rightarrow \phi\phi$ events.

102 layers. Following this idea, tracking studies are performed with additional layers to the
103 baseline configuration of the SciFi detector.

104 A different approach is to give more hit information to the tracking algorithms in order
105 to better discriminate between real and fake tracks. In particular, y information of hits can
106 be retrieved by segmenting the fibres along the y coordinate. This solution, referred in the
107 following as y *segmentation*, and its impact on the tracking performances, is investigated.

108 3.1 y Segmentation

109 The high occupancy in the inner regions of the detector causes higher ghost rates compared
110 to the outer regions, due to more combinations of hits that the tracking algorithms have
111 to handle. The critical dependence of the ghost rate on the occupancy can be shown by
112 characterising its variation with the number of primary vertexes of the event, as presented
113 in Fig. 6 for the forward algorithm. In particular, T-ghosts are exponentially increasing
114 with the occupancy of the detector.

115 In order to mitigate this effect, it might be useful to segment the inner modules of the
116 x -layers along the y direction to reduce the hit ambiguity and the ghost rate. Lower ghost
117 rate will allow to relax the quality requirements used by the tracking algorithms to gain in
118 reconstruction efficiency. However, the y segmentation can only reduce T-ghosts, since
119 it cannot change the effectiveness of the matching procedure with VELO tracks to build
120 long tracks.

121 Due to the high radiation field and increased probability of creating secondary particles,
122 it is not possible to place photodetectors and their supporting infrastructure in the middle
123 of the detector layer, but only on the top and bottom part of the modules. The y
124 segmentation of the SciFi detector can be realised by having double-layered modules where
125 one of the layers has shorter fibres as sketched in Fig. 7. Both layers of the module are
126 readout at the same time, which allows to discriminate the y segment of a hit, as shown
127 in Fig. 8. If a particle intersects the outer part of the module, both full-sized and short
128 fibres would produce a signal which is referred as an *outer hit*. In case of passage of the

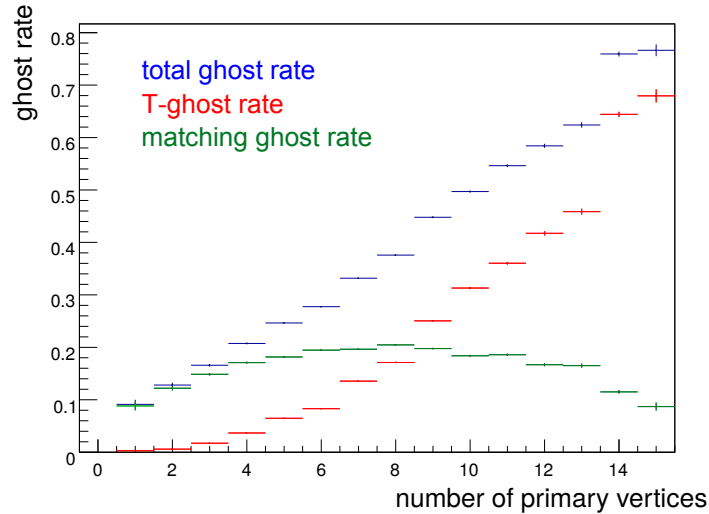


Figure 6: Forward ghost rate dependence versus the number of primary vertices of the event, for matching ghosts (green), T-ghosts (red) and sum of the two contributions (blue).

129 track in the inner part of the module, only the full-sized layer would see a signal, which
 130 corresponds to an *inner hit*. However, when two particles intersect at the same fibre
 131 both inner and outer parts of a segmented module, the signal recorded by the detector is
 132 similar to a single particle intersecting only the outer region. In this case, only the outer
 133 hit is created, reducing the hit efficiency. Furthermore, the addition of extra segmented
 134 modules enhances the multiple scattering due to the increased detector material. In the
 135 most realistic design only two inner modules of two x layers can be segmented in order to
 136 minimize the negative impact of the extra material and hit inefficiency.

137 3.1.1 Simulation

138 The y segmentation of the SciFi layers is simulated by a toy model implemented in the
 139 cluster decoding algorithm, at reconstruction level. For each cluster of the y -segmented
 140 modules, the simulated particles from which it is created are retrieved. If at least one
 141 particle crosses the outer region, the cluster is set to be an outer one. If all the contributing
 142 particles cross the inner region, the cluster is flagged as inner one. If the cluster has no
 143 contributions from hits belonging to simulated particles of the event, for instance in case of
 144 spillover or noise cluster, the region is randomly assigned ignoring any correlation between
 145 occupancy level and noise.

146 3.1.2 Optimization of the tracking algorithms

147 The forward algorithm first uses the y hit information in the preselection step, where hits
 148 from x layers are required to match with hits from stereo planes. The y segmentation
 149 improves the effectiveness of this preselection. A further optimisation is added to the fit

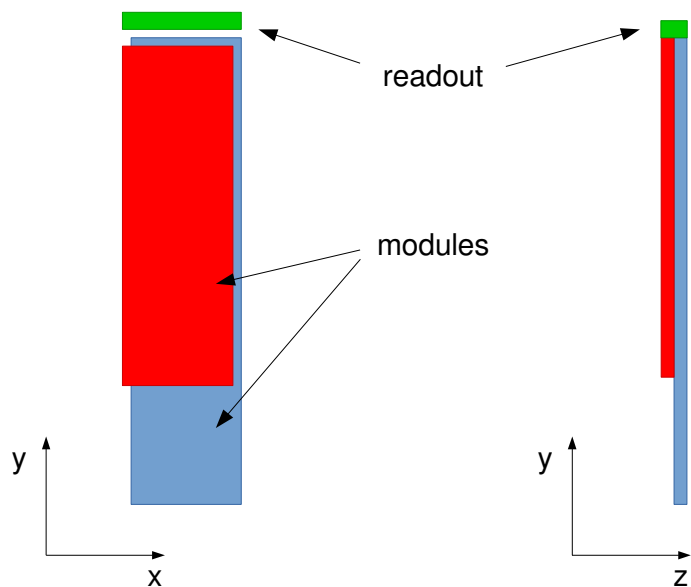


Figure 7: Sketch of SciFi y segmentation, realised by adding modules constituted by shorter fibres in the outer part of the layer.

150 method of track candidates, checking if the hits have y coordinates compatible with the y
 151 projection of the fitted candidate to the segmented layers.

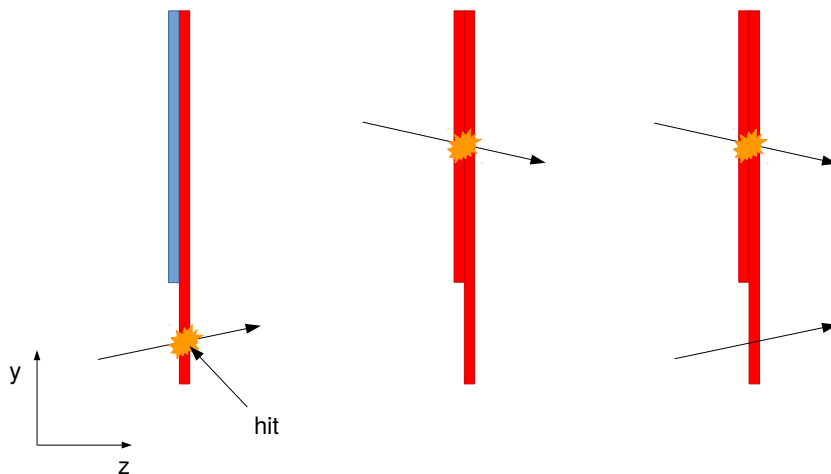


Figure 8: Sketch of SciFi y segmentation readout scheme. When a particle intersects the inner, not segmented part of the module (left), this corresponds to an inner hit. In case of intersection with the outer part of the module (middle), an outer hit is created. When two particles intersect at the same fibre both inner and outer parts of the module, the outer hit only is created.

152 The seeding algorithm determines the full track trajectory from a cubic fit to all hits.
153 Once the trajectory is known, the consistency between the expected y coordinate of the
154 hits and the boundaries of the segmented modules is checked. The x hits that are in the
155 wrong region of the module are removed from the track, and the track is only kept if there
156 are enough hits remaining in it.

157 3.1.3 Results

158 The optimal y segmentation of modules is defined as the absolute value of the y coordinate
159 of the shorter modules for which the tracking efficiency is largest and the ghost rate
160 smallest.

161 Figure 9 shows the results obtained for the forward algorithm with the two inner
162 modules segmented. With higher values of y segmentation, the total ghost rate is first
163 suppressed by about $\approx 10\%$, and then it reaches a plateau where the information of the
164 y coordinate of the hits is no more useful to further decrease ghosts. Over the full y
165 segmentation range, the number of matching ghosts per event is about constant, and
166 only the number of T-ghosts is decreasing, due to the suppression of hit combinatorics
167 caused by the detector segmentation. The tracking efficiency is also decreasing by up to
168 4% for values of the y segmentation of 200 mm, because of the decreasing detector hit
169 efficiency, before finally reaching a plateau. The y segmentation value which assures the
170 best compromise between loss of efficiency and decreasing of ghost rate is chosen to be
171 150 mm, also accordingly to the seeding studies shown in the next paragraphs.

172 In Table 2 the forward results with baseline SciFi detector, and with y segmentation
173 equal to 150 mm, are summarised. The total ghost rate is decreasing by 8%, mainly
174 due to the strong reduction of T-ghosts. However, the tracking efficiency significantly
175 decreases for all types of tracks, due to the missing hits in the inner parts of the y
176 segmented modules coming from particles crossing the same fibres in the outer region.
177 To recover the efficiency, the hit requirements in the forward algorithm are then relaxed:
178 the reconstruction efficiencies for long tracks and long tracks of high momentum from
179 B mesons are now almost recovered, but with higher ghost rate with respect to the not
180 segmented SciFi detector. Concluding, the implementation of the SciFi y segmentation
181 currently studied is not giving any benefits to the forward reconstruction in terms of
182 tracking efficiency and ghost rate, with respect to the baseline SciFi detector.

183 Table 3 lists the performance of the seeding algorithm for long and high momentum
184 long tracks. Only a small gain in efficiency is seen due to the hit inefficiency introduced
185 by y segmentation. Depending on the number of layers segmented, 2% to 9% reduction in
186 ghost rate is seen.

187 3.2 Additional x layers

188 As already mentioned in section 3.1, it is crucial to add extra detector material only
189 where this can improve the reconstruction performances on particles of physics interest,
190 because of the increasing multiple scattering effects due to the material. In particular,

hit requirements	no y segmentation default	y seg = 150 mm default	y seg = 150 mm reduced
long	83.8%	80.4%	83.4%
long $p > 5$ GeV/ c	92.1%	86.5%	88.9%
long $p > 5$ GeV/ c , from B	94.5%	91.1%	93.2%
total ghost rate	35.9%	27.9%	36.3%
matching ghosts/event	23.1%	23.7%	26.7%

Table 2: Forward performances with baseline SciFi detector and default hit requirements (minimal number of x hits equals 4 and minimal total number of hits equals 10) used in the reconstruction, and y segmentation equal to 150 mm with reduced hit requirements (minimal number of x hits equals 3 and minimal total number of hits equals 9). The results are computed over a sample of 5000 simulated $B_s \rightarrow \phi\phi$ events.

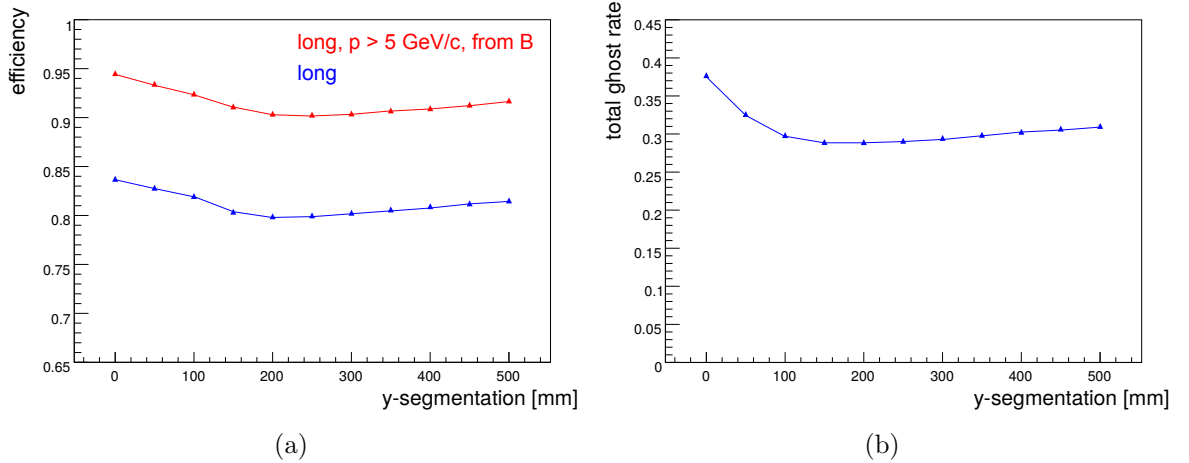


Figure 9: Forward performances with two inner modules segmented. a) Reconstruction efficiency for long tracks (blue) and long tracks with momentum greater than $p > 5$ GeV/ c coming from B meson decays, depending of the y segmentation value. b) Total ghost rate versus y segmentation.

191 the inner region of the SciFi, nearest to the beam pipe, is intersected by the majority
192 of B meson daughters, and has the highest particle occupancy of the detector, where
193 the availability of more hits can improve the track reconstruction. This is why the most
194 preferable configuration of extra layers considers the addition of two inner modules only.

195 3.2.1 Simulation

196 A full-detailed simulation is realised creating custom geometries which include the extra
197 layers, starting from the geometry databases describing the SciFi detector in the LHCb
198 simulation framework. Both generation and digitisation simulations have to be modified

	long	long, $p > 5 \text{ GeV}/c$	ghost rate
no y segmentation	90.5%	94.0%	18.3%
2 segmented x layers			
100 mm	+0.70%	+0.60%	+0.60%
150 mm	+0.70%	+0.50%	-0.80%
200 mm	+0.70%	+0.60%	-1.50%
250 mm	+0.80%	+0.60%	-1.90%
300 mm	+0.80%	+0.60%	-2.00%
3 segmented x layers			
100 mm	+0.70%	+0.50%	-1.40%
150 mm	+0.70%	+0.40%	-3.40%
200 mm	+0.70%	+0.40%	-4.40%
250 mm	+0.70%	+0.50%	-4.70%
300 mm	+0.80%	+0.50%	-4.60%
6 segmented x layers			
100 mm	+0.60%	+0.30%	-5.10%
150 mm	+0.50%	+0.10%	-8.00%
200 mm	+0.50%	+0.00%	-9.10%
250 mm	+0.60%	+0.20%	-9.20%
300 mm	+0.60%	+0.20%	-8.60%

Table 3: The performance of the seeding algorithm for different scenarios of y -segmented modules.

199 according to the modified number of SciFi layers. In this detailed simulation, all digitisation
200 effects are simulated for extra layers such as for standard planes.

201 Several geometries were tested in order to find, within the given engineering and infras-
202 tructural constraints, the optimal configuration of the extra layers for which the maximum
203 improvement in tracking performances can be obtained. The optimal configuration found
204 is characterised by two extra layers with inner modules only, positioned right behind the
205 first station and the second one, as shown in Fig. 10. This geometry will be referred in the
206 following as UFT 5x5, to discriminate it from the baseline SciFi geometry, called UFT 5x.
207 For cross check purposes, a geometry version with full-sized additional layers is studied
208 too, named UFT 5x6.

209 3.2.2 Forward algorithm optimisation and performances

210 The structure of the forward algorithm is based on the idea of track reconstruction using
211 a homogeneous detector; one of the most important consequences is the expectation for

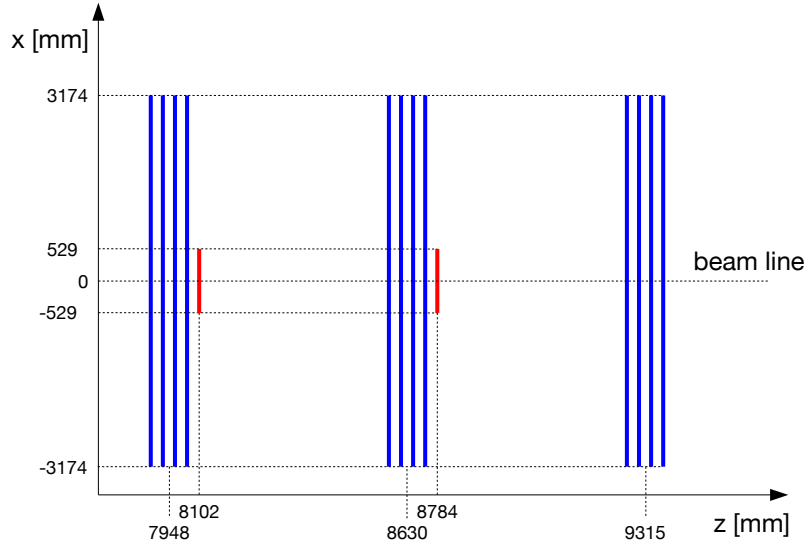


Figure 10: Sketch of the UFT 5x5 geometry, characterised by two extra layers (in red) with inner modules only. Standard layers are blue coloured. Only layer dimensions along the x coordinate are drawn to scale.

212 track candidates having the same number of hits. This idea is widely used in the algorithm,
 213 mainly for comparing multiple candidates of a single VELO track projection.

214 This geometrical assumption is no longer valid when adding extra layers consisting of
 215 inner modules only. In this case, the reconstruction algorithm has to distinguish between
 216 candidates which are expected to intersect or not the additional layers. In fact, to fairly
 217 compare tracks which are expected to geometrically intersect different number of planes,
 218 threshold values used for the reconstruction have to be differentiated. In particular,
 219 higher thresholds must be used for candidates which intersect the extra layers.

220 In the Hough-like clustering of hits, the extra layer boundaries are projected to the
 221 reference plane, according to the transformation defined by the extrapolated VELO track.
 222 Clusters of hits with an x projection compatible with included in the projected area of
 223 the additional layers, are flagged as expected to intersect extra layers. A more precise
 224 evaluation is performed after a fit of the full track. Finally, a quality factor is computed
 225 for each of the fitted track candidates, based on the number of expected intersected layers.
 226 This factor is then used at the final stage of the event reconstruction, to filter ghost tracks.

227 To improve the rejection of noise or combinatorial hits in the preselection step, x hits
 228 already matched with stereo ones can be additionally matched to x hits from extra layers.
 229 This matching uses a search window tighter than the one used for stereo hits. For each hit
 230 of an x layer within the x window search, a matching with both the nearest stereo and
 231 extra layer is required. This will be referred in the following as *triplet hit matching*, to be
 232 distinguished from the *doublet* case where a matching with hits from extra layers is not
 233 required.

234 To correctly implement *triplet* hit matching in the forward preselection stage, the

235 working point of this method is determined by computing the discrimination power for
 236 *good hits* with respect to the others. In particular, a hit efficiency is defined by counting
 237 how many of the available x hits, which belong to the generated particle, passed the
 238 preselection; all other hits are defined as background. Values of preselection efficiency
 239 versus background rejection are computed varying the search windows for both triplet and
 240 doublet hit matching, as shown in Fig. 11. An x tolerance of 2 mm is chosen as working
 241 point for the *triplet* matching. This value is used for the results which follow.

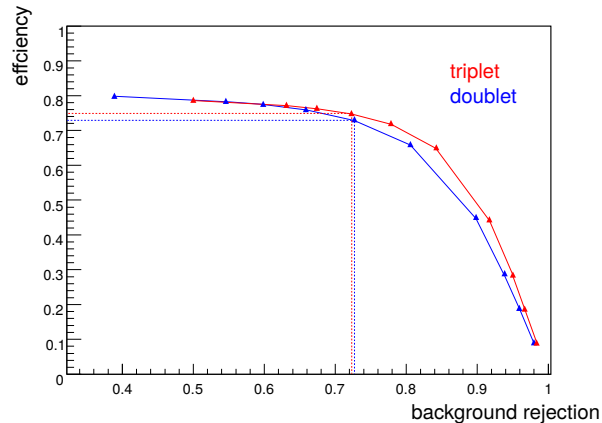


Figure 11: Forward preselection efficiency on hits selected by *doublet* (blue) or *triplet* (red) hit matching, versus hit background rejection. The blue dashed lines indicate the default working point for *doublet* matching, the red dashed the working point chosen for *triplet* matching.

242 It is also required to determine the new working point of the reconstruction algorithm
 243 on a geometry different than the baseline one. The four main parameters related to the
 244 number of hits required in the different stages of the forward algorithm are investigated:

- 245 - *MinTotalHits*: minimum number of hits required for a candidate track;
- 246 - *MinXHits*: minimum number of x hits required for a single Hough cluster;
- 247 - *MinXPlanes*: minimum number of x planes which have to be intersected, in a single
 248 Hough cluster;
- 249 - *MinXSinglePlanes*: minimum number of x planes which have to be intersected by a
 250 single hit, in a single Hough cluster.

251 Figure 12 shows the forward performances obtained for the UFT 5x6 geometry with
 252 full-sized extra layers, compared to the baseline UFT 5x geometry, for different sets of
 253 hit requirements. Exploiting the full-sized extra layers, with nominal SciFi hit efficiency
 254 it is possible to gain about 2% of tracking efficiency on long tracks, and about 1% on
 255 long tracks of high momentum which come from B meson decays, with a total ghost rate
 256 lower by about 1% with respect to the baseline SciFi geometry. Furthermore, it is useful

257 to explore the performance, which can be obtained simulating additional hit inefficiency
 258 of the SciFi detector. A spatially uniform hit inefficiency is added, randomly removing
 259 a certain amount of SciFi clusters during the hit decoding phase of the reconstruction
 260 algorithm. In Fig. 12 the Forward performances are reported, simulating an extra 3%
 261 and 5% hit inefficiency. In both cases, assuming to keep the same total ghost rate of the
 262 scenario with nominal SciFi hit efficiency, the UFT 5x6 geometry assures a gain of about
 263 3-4% on tracking efficiency for long tracks, and of about 1% for long tracks from B mesons
 264 with $p > 5 \text{ GeV}/c$.

265 In Fig. 12 the forward performances of the baseline UFT 5x geometry is compared
 266 to the UFT 5x5 geometry with extra layers consisting of inner modules only. In this
 267 scenario, the addition of inner modules does not improve the performances of the forward
 268 algorithm. Further studies show that, for the current algorithm, the extra information
 269 coming from layers with inner modules only is not fully exploited to increase the signal-
 270 over-background hit ratio, that indeed remains almost constant for this detector region.
 271 All the optimisations studied to take advantage of the extra inner modules are not enough
 272 to better discriminate signal hits from background ones, especially for the inner detector
 273 region where the particle rate and density, and consequently the noise and spillover hit
 274 rates, are the highest. This is also related to the fact that the forward algorithm was
 275 originally designed to reconstruct particles intersecting a tracker consisting of identical
 276 and uniform detector layers. This design is not optimal to profit from the addition of
 277 non-full-sized layers.

278 3.2.3 Seeding algorithm adaptation and performances

279 The addition of two extra x -layers makes necessary to re-evaluate how to set the parameters
 280 of the seeding algorithm as well. On one hand, all the parameters related to the number
 281 of hits that a track candidate should contain must be adjusted. This includes both the
 282 number of x -hits and the number of the stereo-hits. Those parameters are *MinXPlanes*
 283 and *MaxNHits*, which govern the number of hits for the track candidates, as well as all
 284 the *MinUV* parameters, which relate the size of the xz -projection to the minimum number
 285 of required stereo-hits. Overall, there are 17 such parameters, since the seeding algorithm
 286 has 3 independent iterations for different momentum ranges sequentially.

287 On the other hand, the performance of the algorithm could improve by tweaking the
 288 other parameters sensibly. For this reason, a step-by-step profiling of the performance of
 289 the seeding algorithm is carried out in order to identify potential bottlenecks and to show
 290 which parameters may need adjusting. This shows, notably, that the additional layers
 291 help in keeping the ghost rate under control. So, it is possible to relax the conditions
 292 under which a hit belonging to a reconstructed track is removed from the pool of available
 293 hits for the following iterations of the algorithm. This removal procedure, called *flagging*,
 294 has a great impact on both ghost rate and timing. The relevant parameter that needs
 295 tuning in this context is the *SizeToFlag* parameter, which controls the number of hits that
 296 a reconstructed track must contain in order for its hits to be *flagged*.

297 Specifically for the UFT 5x5 geometry, it is necessary to include a check on the number

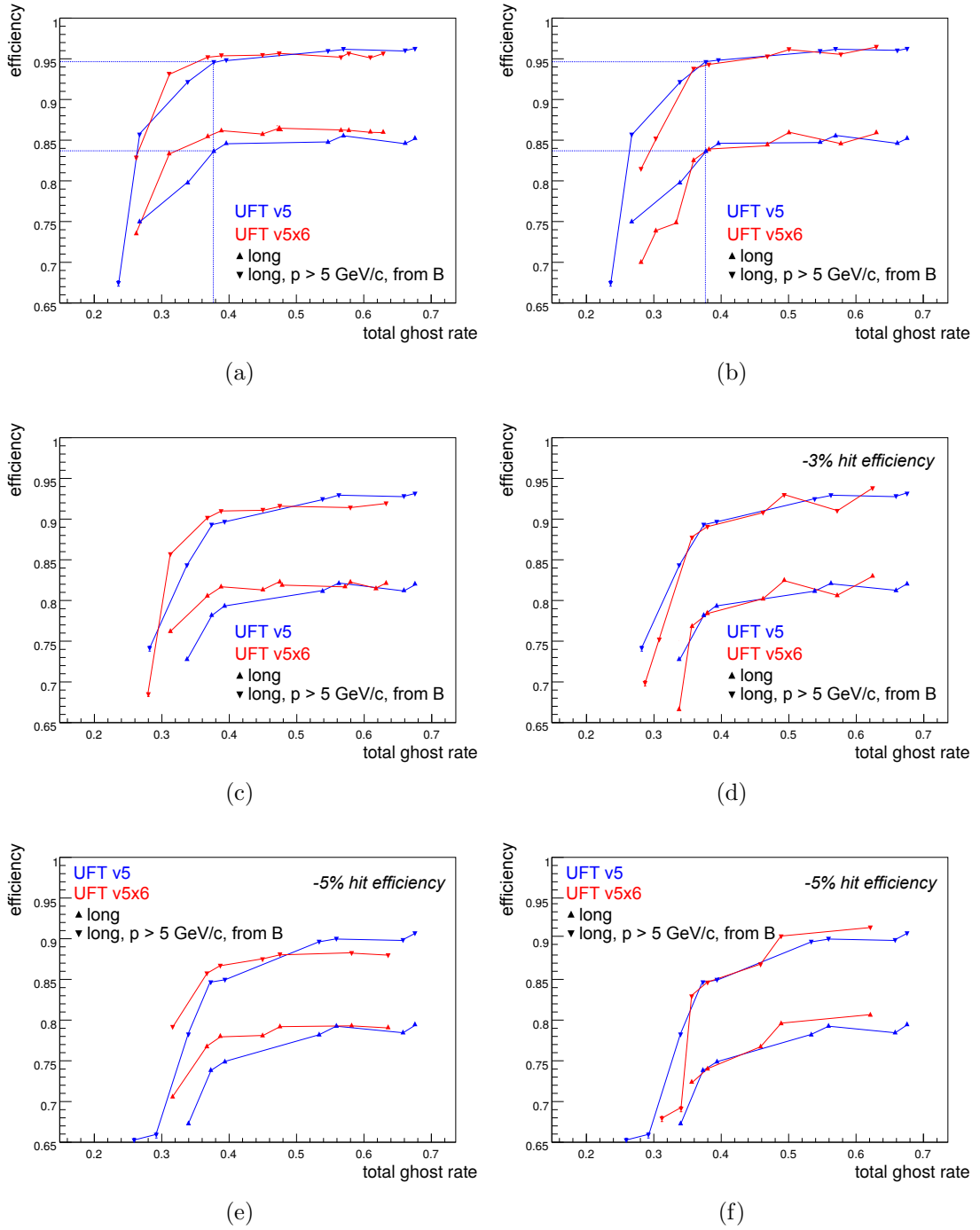


Figure 12: Comparison of forward reconstruction efficiency for long tracks and long tracks from B mesons with $p > 5$ GeV/ c , on standard (blue) and geometries with extra layers (red). In left column, additional layers are full sized while for right column they only contain two inner modules. Each point corresponds to a set of hit requirements used in the reconstruction corresponding to the ghost rate in the x -axis. Results are for standard hit efficiency of the SciFi detector (top), and with additional hit inefficiency of 3% (middle) and 5% (bottom). The dashed blue lines indicate the performances for the standard reconstruction on the UFT 5x6 geometry.

298 of x -layers effectively crossed by the track candidate. This check is made during the
299 xz -projection search as soon as the trajectory for the candidate is determined by using a
300 cubic model and a triplet of hits. Depending on the result of this check, the algorithm
301 adjusts all its parameters to one of the 3 possible configurations (corresponding to 6, 7 or
302 8 x -layers crossed).

303 In both alternative geometries, we also investigate the performance of the seeding when
304 only the additional x -layer in the first station is active.

305 Unsurprisingly, the additional information given by the 2 extra x -layers allows for
306 an improvement on the quality of the xz -projection candidates. A consequence of this
307 improvement is that the other steps of the seeding algorithm are now less CPU-intensive,
308 which brings down the overall run time of the seeding algorithm by a factor ~ 2 for the
309 UFT 5x6 geometry and ~ 1.6 for the UFT 5x5 geometry. This reduction of the execution
310 time is valuable since the algorithm will be run online at the trigger level.

311 The performance of the reconstruction improves for both alternative geometries: the
312 ghost rate decreases when the number of active additional layers increases, while the
313 efficiency improves or stays the same for every track category when compared to the 12
314 layers baseline.

315 It is interesting to note that, due to the discrete nature of the handle on the parameters
316 of the algorithm, the optimal configurations for 13 active layers exhibit overall efficiencies
317 on the same level and a slightly worse ghost rate if compared to the 14 active layer ones.
318 The detailed performance for both geometries is shown in Table 4.

319 **3.3 Beam hole and layer size**

320 The beam hole shape and dimension, such as the layer size, are of crucial relevance to both
321 SciFi engineering and tracking performances. The beam hole region is characterised by
322 the highest particle density, with the maximum located on the beam itself, progressively
323 decreasing towards the outer region of the SciFi layers. A wider beam hole, cutting away
324 portions of the central region of the detector, can in principle assure a lower ghost rate
325 and less critical degradation of the detector due to the particle irradiation. On other
326 hand, fewer particles will intersect the detector, resulting in a smaller yield of particles.
327 Vice versa, with a smaller beam hole the ghost rate is expected to get worse, but the
328 particles that potentially can be reconstructed increase. The exact shape of the beam hole
329 is important for engineering, as it defines how easy it is to build the inner modules. A
330 circular hole would be ideal as that would allow to cover the full acceptance, however, this
331 is considered not feasible to construct. Three different beam holes are studied, sketched in
332 Fig. 13:

- 333 - *symmetric rectangle*: gives the highest acceptance of the detector, which requires
334 two modules per layer which have a cutout. This cutout has different dimensions for
335 x layers and for stereo layers;
- 336 - *asymmetric rectangle*: also has two central modules per layer, but the dimensions of
337 the cutout are the same for x layers and stereo layers. This option has the drawback

	12 active layers	13 layers, UFT 5x6	14 layers, UFT 5x6	13 layers, UFT 5x5	14 layers, UFT 5x5
ghost rate	18.4%	16.4%	15.1%	16.2%	15.1%
long	89.9%	91.1%	91.3%	90.2%	89.9%
long, $p > 5 \text{ GeV}/c$	94.5%	95.1%	95.0%	94.8%	94.6%
long from B , $p > 5 \text{ GeV}/c$	94.9%	95.7%	95.6%	95.3%	94.9%
noVelo	87.6%	90.3%	90.7%	88.0%	87.7%
noVelo, $p > 5 \text{ GeV}/c$	94.2%	95.9%	95.7%	94.4%	94.3%
noVelo from DB, $p > 5 \text{ GeV}/c$	93.1%	98.1%	96.9%	94.4%	93.8%

Table 4: The performance of the seeding algorithm for the geometries UFT 5x6 (2 full additional x -layers) and UFT 5x5 (2 partial additional x -layers) over 1000 $B_s \rightarrow \Phi\Phi$ simulated events. The efficiencies are shown for long tracks and tracks not having a VELO component (these tracks can not be reconstructed with the forward algorithm). The gain in performance is clear already with only 1 active additional layer. The activation of the second additional layer mostly allows for an improvement in the ghost rate while the efficiencies slightly degrade.

338 of a smaller acceptance compared to the symmetric case;

339 - *large symmetric rectangle*: has only one special module per layer, which has the same
340 dimensions for x layers and stereo layers. This option has the worst acceptance.

341 For all configurations, the beam hole has same dimensions for each of the three SciFi
342 stations. The minimum clearance to the beam pipe is 20 mm for the last station.

343 Finally, the layer size defines the SciFi geometrical acceptance, and must fulfill the
344 geometrical constraints of the detector infrastructures. The baseline geometry in the
345 simulation consists of 12 modules for all SciFi layers, and an alternative geometry with
346 10 modules only for the first two stations (T1, T2) and 12 modules for the last one (T3).
347 The alternative geometry is sketched in Fig. 14. It correctly fits within the infrastructure
348 design, remaining within the nominal geometrical acceptance of the LHCb detector of 300
349 mrad on the bending plane.

350 3.3.1 Simulation

351 The studies on optimised beam hole and layer geometry are first performed by removing
352 hits from the baseline geometry. During the hit decoding stage of the tracking algorithms,

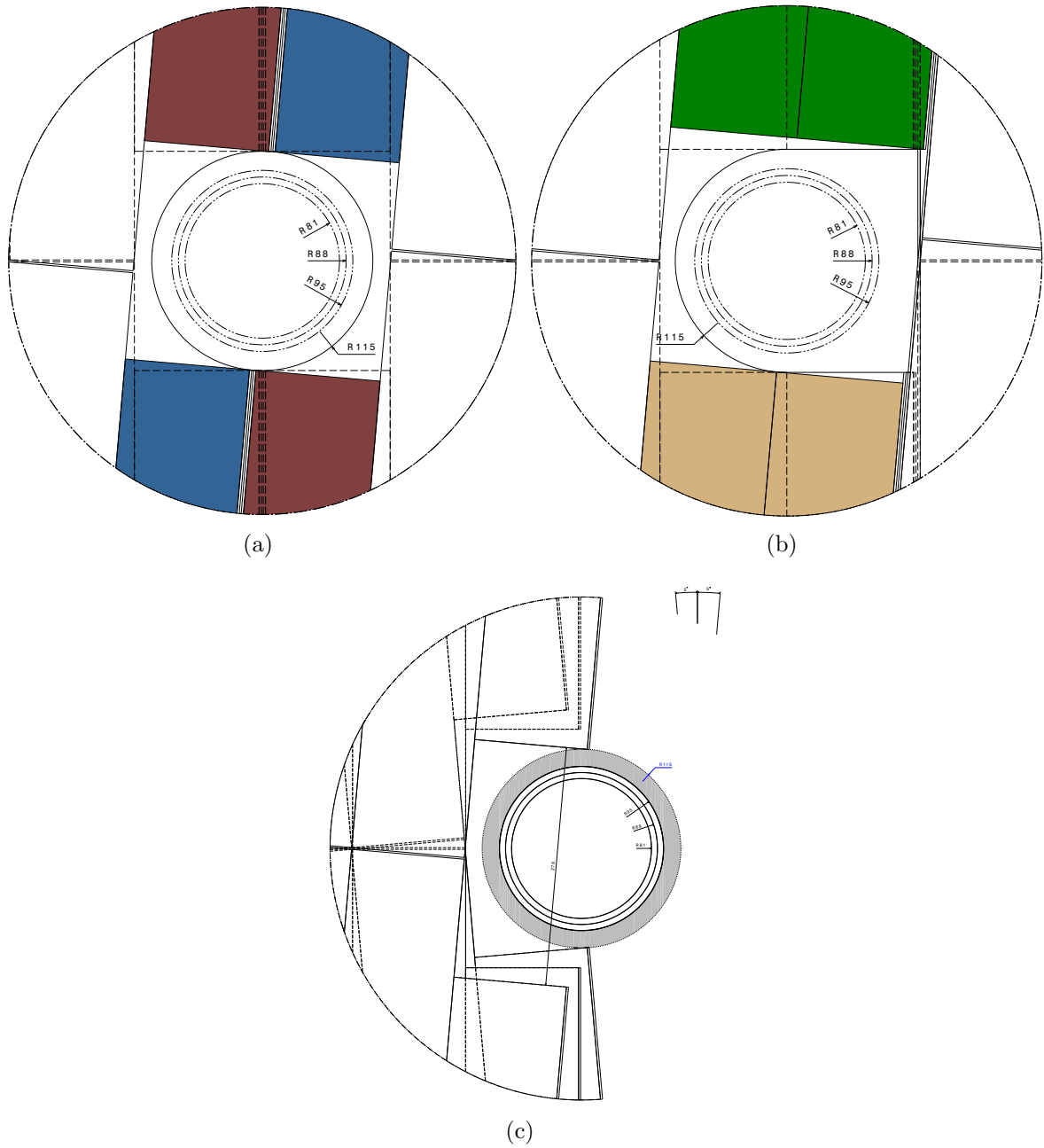


Figure 13: Sketches of the symmetric rectangular (a), asymmetric rectangular (b) and symmetric, large rectangular (c) beam holes.

353 the new beam hole region is defined, and all hits falling in that region are deleted. The
 354 standard reconstruction follows, such as the redefinition of reconstructible particles basing
 355 on the new hit contents of the event, and the matching of reconstructed tracks with the
 356 simulated particles.

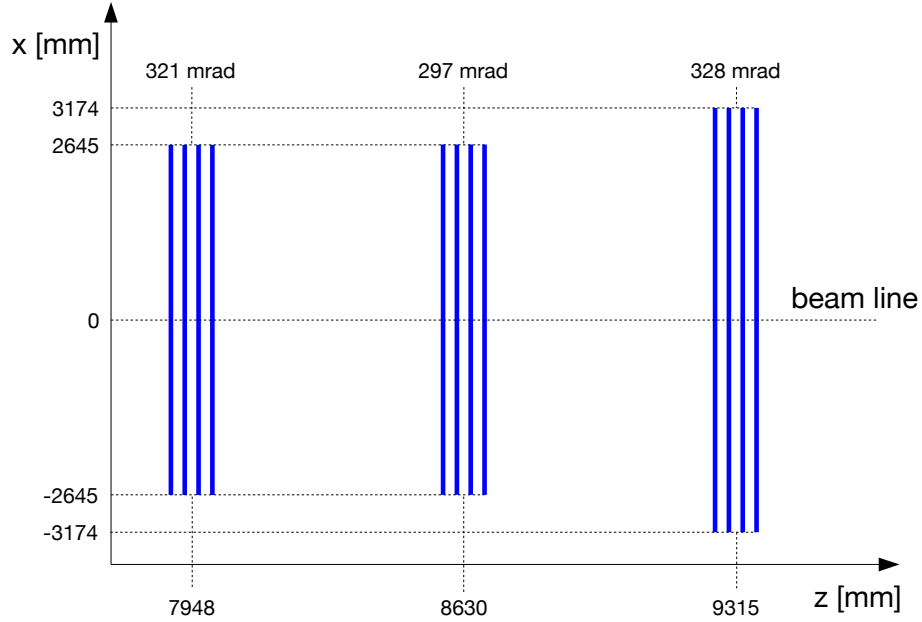


Figure 14: Sketch of the SciFi geometry having T1 and T2 stations constituted by 10 modules, and T3 by 12 modules. The values of the maximum angular acceptance along the xz plane are reported for the three stations. Only layer dimensions along the x coordinate are drawn in scale.

357 Note that with this toy implementation, custom beam holes can only be compared
 358 with a smaller hole, since hits can only be removed. For this reason, all toy studies are
 359 performed starting from samples generated with the UFT 2x geometry, which has a circular
 360 beam hole of minimal dimensions as sketched in Fig. 15. As reference, the beam hole
 361 implemented in the baseline UFT 5x geometry is used.

362 Two new geometries are created for the full simulation, based on the UFT 5x geometry,
 363 to validate the toy results. The so-called UFT 5x8 geometry implements the small
 364 symmetric rectangular hole previously described. The UFT 5x9 geometry also includes
 365 the reduced layer size, in addition to this rectangular hole.

366 3.3.2 Results

367 The resulting number of reconstructible particles obtained for the previously described
 368 beam holes are summarised in Table 5, and for the case of 10 modules in station T3.
 369 The results are compared with the ideal circular hole having constant radius 105 mm for
 370 all the stations, to assure a clearance of 20 mm to the beam pipe for the third station.
 371 For reference, the UFT 2x and UFT 5x beam holes are also simulated and added to the
 372 comparison. For wider beam holes, high-momentum particles show a more pronounced
 373 drop in reconstructability with respect to low momentum ones. This is expected, because
 374 of the increasing co-linearity of particles with the beam line, as the momentum increases.
 375 Removing the two outer modules from the first and second stations, about 0.7% of long-

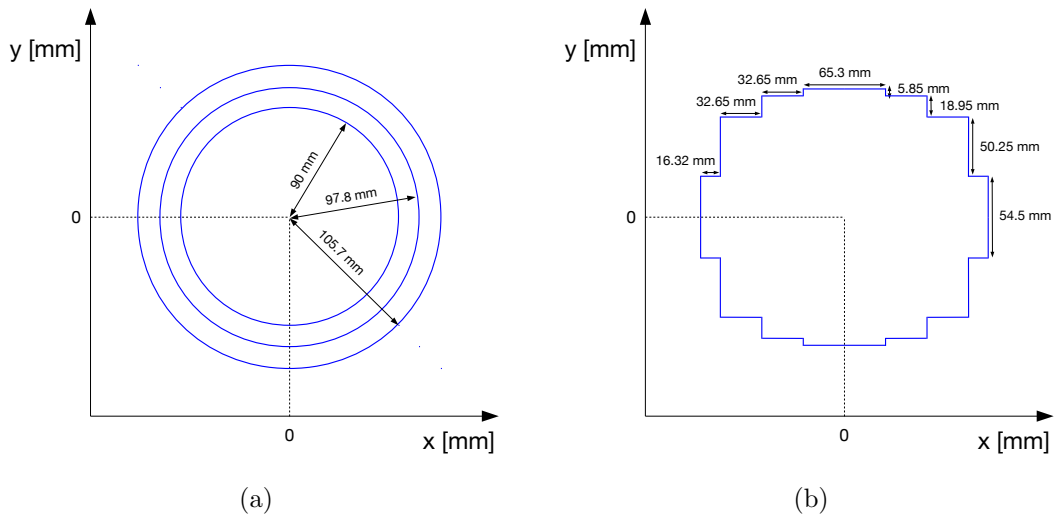


Figure 15: a) Sketch of the circular beam hole implemented in the UFT 2x geometry, with radius increasing from $r_1 = 90 \text{ mm}$ of the first station to $r_3 = 105.7 \text{ mm}$ of the third one. b) Sketch of the step beam hole implemented in the UFT 5x geometry for the first station. The hole dimensions gradually increase for the second and third stations.

376 reconstructible particles are lost, and about 0.3% of long-reconstructible particles having
 377 $p > 5 \text{ GeV}/c$ and coming from B meson decays. This is because low momentum particles
 378 are more bent by the LHCb magnetic field, and consequently they have more hits on the
 379 outer layer modules with respect to high-momentum particles.

380 Table 6 shows the forward tracking performances for all the beam hole scenarios. The
 381 tracking efficiency is slightly reducing for wider holes for a maximum factor of 0.4%, and
 382 the total ghost rate is decreasing of about 3.5% because of the removal of hits in the most
 383 busy detector region, around the beam pipe. However, these represent conservative results,
 384 since the radiation damage is overestimated for wider holes when the attenuation maps
 385 to simulate irradiation resulting from the UFT v2 circular hole are used. This results in
 386 higher attenuation of the reflected photons, thus decreasing the effective hit efficiency of
 387 the detector which has a direct impact on the reconstruction efficiency.

388 Table 7 shows the variation of number of reconstructible particles for the full geometries
 389 UFT 5x8 and UFT 5x9, compared to the baseline UFT 5x. These results show the same
 390 trends as summarised in Table 5 for the toy model. In particular, the loss of reconstructible
 391 particles due to the removal of the outer modules from the first two stations, obtained
 392 as difference of the UFT 5x8 and UFT 5x9 results, confirms the toy results. However, a
 393 discrepancy of 0.4 – 0.5% is observed for the variation on the number of reconstructible
 394 particles with the symmetric hole simulated by the full geometries, and the results of the
 395 toy model. This difference can be related to the large per-event fluctuations on the number
 396 of reconstructible particles observed by simulating independent samples, or to some effect
 397 not taken in account by the toy study. Anyhow, it is expected that this behaviour affects

	long	long, $p > 5 \text{ GeV}/c$	long, $p > 5 \text{ GeV}/c$, from B
	full-sized layers		
UFT 2x circle	+1.05%	+1.54%	+1.03%
symmetric	-0.68%	-1.81%	-1.48%
asymmetric	-1.03%	-2.38%	-1.71%
large symmetric	-1.92%	-3.38%	-2.41%
UFT 5x step	+0.16%	+0.09%	+0.11%
	T1-T2: 10 modules, T3: 12 modules		
UFT 2x circle	+0.35%	+1.42%	+0.78%
circular $r = 115 \text{ mm}$	-0.70%	-0.32%	-0.34%
symmetric	-1.39%	-2.30%	-1.81%
asymmetric	-1.68%	-2.69%	-2.07%
large symmetric	-2.60%	-3.80%	-2.77%

Table 5: Percentage variation of the number of reconstructible particles for different beam hole shapes and layer sizes simulated by the toy model, with respect to the ideal circular beam hole having radius $r = 115 \text{ mm}$ and all layers 12 modules sized. The results are computed over a MC sample of 17000 simulated $B_s \rightarrow \phi\phi$ events.

T1-T2: 10 modules, T3: 12 modules			
	long	long, $p > 5 \text{ GeV}/c$, from B	total ghost rate
circular $r = 115 \text{ mm}$	81.0%	91.8%	38.9%
symmetric	80.8%	91.7%	35.6%
asymmetric	80.6%	91.6%	35.2%
large symmetric	80.6%	91.5%	35.1%

Table 6: Forward tracking efficiency and ghost rate for different beam hole shapes simulated by the toy model, compared to the ideal circular beam hole having radius $r = 115 \text{ mm}$. The results are computed over a sample of 17000 simulated $B_s \rightarrow \phi\phi$ events.

398 almost equally the other geometries too, not affecting the overall conclusions of the studies.

399 The performances for the UFT 5x8 and 5x9 geometries are summarised in Table 8.
400 With respect to the baseline UFT 5x geometry, the tracking efficiency remains almost
401 constant, and a drop of $\approx 3\%$ for the total ghost rate is observed, confirming the toy
402 results.

	long	long, $p > 5 \text{ GeV}/c$	long, $p > 5 \text{ GeV}/c$, from B
toy 5x step hole \rightarrow toy symmetric hole	-0.84%	-1.90%	-1.59%
UFT 5x \rightarrow UFT 5x8	-1.39%	-2.37%	-1.98%
UFT 5x \rightarrow UFT 5x9	-2.17%	-2.86%	-2.34%

Table 7: Percentage variation of the number of reconstructible particles for UFT 5x8 and UFT 5x9 geometries compared to the baseline UFT 5x obtained with the full simulation, and for the symmetric hole compared to the UFT 5x one simulated by the toy model. The results are computed over samples of 5000 simulated $B_s \rightarrow \phi\phi$ events.

	long	long, $p > 5 \text{ GeV}/c$, from B	total ghost rate
UFT 5x	83.5%	94.2%	36.2%
UFT 5x8	83.6%	94.6%	32.9%
UFT 5x9	83.5%	94.4%	33.1%

Table 8: Forward tracking efficiency and ghost rate for UFT 5x8 and UFT 5x9 geometries, compared to the baseline UFT 5x. The results are computed over MC samples of 5000 simulated $B_s \rightarrow \phi\phi$ events.

4 Conclusions

403

404 Studies have been performed to optimize the SciFi detector layout, in order to improve
405 the performances of the tracking algorithms. Two possibilities are investigated: a y
406 segmentation and the addition of more layers in the high occupancy regions of the detector.
407 In both cases only a minor performance boost is observed in the seeding algorithm while
408 the forward algorithm performs either the same or worse. Considering additional material
409 and complexity introduced without significant gain, we do not recommend either of the
410 two options.

411 Additional studies have been performed to estimate the acceptance loss due to changes
412 in the beam hole shape and layer size. A rectangular beam hole and reduced layer size in
413 the first and second stations is accepted as default with minimal loss in acceptance while
414 allowing easier hardware installation and development.

415 References

- 416 [1] LHCb collaboration, A. A. Alves Jr. *et al.*, *The LHCb detector at the LHC*, JINST **3**
417 (2008) S08005.
- 418 [2] LHCb collaboration, R. Aaij *et al.*, *LHCb detector performance*, Int. J. Mod. Phys.
419 **A30** (2015) 1530022, [arXiv:1412.6352](#).
- 420 [3] LHCb collaboration, R. Aaij *et al.*, *Framework TDR for the LHCb Upgrade: Technical*
421 *Design Report*, CERN-LHCC-2012-007. LHCb-TDR-012.
- 422 [4] L. Del Buono, O. Gruenberg, and D. Milanés, *Geometry of the Scintillating Fiber*
423 *detector*, LHCb-PUB-2014-005. This note describes the planned dimensions of the
424 detector at the time of the optimization study.
- 425 [5] LHCb collaboration, R. Aaij *et al.*, *LHCb Tracker Upgrade Technical Design Report*,
426 CERN-LHCC-2014-001. LHCb-TDR-015.
- 427 [6] Y. Amhis, O. Callot, M. De Cian, and T. Nikodem, *Description and performance*
428 *studies of the Forward Tracking algorithm for a scintillating fibre detector at LHCb*,
429 LHCb-PUB-2014-001.
- 430 [7] Y. Amhis, P. Billoir, F. Polci, and R. Quagliani, *The Hybrid Seeding algorithm for a*
431 *scintillating fibre detector at LHCb: description and performances*, LHCb-PUB-2017-
432 018.